J Mater Sci (2009) 44:843–848
DOI 10.1007/s10853-008-3132-x

Dense spinel $MnCo_2O_4$ film coating by aerosol deposition on ferritic steel alloy for protection of chromic evaporation and low-conductivity scale formation

Jong-Jin Choi · Jungho Ryu · Byung-Dong Hahn · Woon-Ha Yoon · Byoung-Kuk Lee · Dong-Soo Park

Received: 10 June 2008 / Accepted: 24 November 2008 / Published online: 11 December 2008

Abstract Conducting ceramic layers with a spinel structure of $MnCo_2O_4$ and a thickness of ~3 μm were deposited on ferritic stainless steel (SS) by aerosol deposition (AD), for use as an oxidation-resistant coating layer on the metallic interconnects of a solid oxide fuel cell (SOFC). The microstructural changes in the interface between the $MnCo_2O_4$ and SS were analyzed, as were the subsequent electrical conductivity changes at an SOFC operating temperature of 800 °C in air. The coated spinel layers were dense without pores or cracks, and maintained good adhesion even after oxidation at 800 °C for 1,000 h in air atmosphere. Close observation of the interface between the coated spinel oxide and SS substrate indicated the presence of ~1-μm thick, Cr-rich scale formation; however no $MnCrCoO_4$ or $MnCr_2O_4$ spinel phase was detected. The area specific resistance (ASR) of the $MnCo_2O_4$-coated alloy after heat treatment at 800 °C for 1,000 h was 13.4 mΩ cm^2.

Introduction

The solid oxide fuel cell (SOFC) stack consists of various ceramic constituents, whereas oxidation-resistant metal alloys are the most promising candidates for interconnects in the planar SOFC system [1, 2]. Among the metal alloys, chromia formation alloys, especially ferritic stainless steels (SSs), are preferred because of their electrically conducting oxide scale formation, appropriate thermal expansion coefficient, excellent formability, and low cost [3, 4]. However, the scale-forming chromia formation alloys have high Cr volatility. Recently developed alloys such as Crofer22 APU form a $(Mn,Cr)_3O_4$ spinel top layer and a Cr-rich sublayer, and may have lower volatility of Cr from spinel than from chromia. Nevertheless, the Cr volatility from the Cr-containing spinel still causes an unacceptable degradation in cell performance [5, 6].

An alternative solution is to form a protection layer with high electrical conductivity and low Cr diffusivity on the Cr-based alloys. Protection layers that have been extensively reported are perovskite structure conducting ceramics coatings such as Sr-doped lanthanum manganite and ferrite, which are often used as cathode materials in the SOFC stack [7–10]. The potential problems of these conducting ceramics coatings are chromium cation diffusion through the coatings and related thermochemical stability of the coating layer during thermal cycling. Recently, Yang et al. investigated spinel layers coatings by slurry coating of $Mn_{1.5}Co_{1.5}O_4$ powder on specially prepared SS (Crofer22 APU) [11]. The coated sample showed excellent long-time electrical and structural stability. However, the films made with these methods were rather porous and required sintering at high temperature which can induce unexpected surface oxidation.

Recently, our research group succeeded in depositing highly dense, thick, conducting perovskite structure ceramics ($La_{0.8}Sr_{0.2}MnO_3$, LSM) on ferritic SS by using the aerosol deposition (AD) process, and demonstrated the potential use in real applications [12]. The AD process is a room-temperature operating powder consolidation method for the formation of a thick and dense ceramic layer, based on the impact adhesion of fine particles. AD process has a

J.-J. Choi (✉) · J. Ryu · B.-D. Hahn · W.-H. Yoon · B.-K. Lee · D.-S. Park
Functional Ceramics Research Group, Department of Powder Materials, Korea Institute of Materials Science, 531 Changwondaero, 641-831 Changwon, Gyeongnam, South Korea
e-mail: finaljin@kims.re.kr

very high deposition rate (>10 μm/min) and requires no additional heating for solidification of the ceramic powder [13, 14]. The coated layers were highly dense without pores or cracks, and maintained good adhesion even after oxidation at 800 °C for 1,000 h in air atmosphere. However, the area specific resistance (ASR) value of the LSM-coated alloy increased steadily, presumably due to formation at the interface of $MnCr_2O_4$ phase which has an electrical conductivity similar to that of Cr_2O_3 and about three orders of magnitude lower than that of $MnCo_2O_4$ [15]. Since $MnCo_2O_4$ is known to not only have high electrical conductivity but also reduce Cr interdiffusion from Cr-containing alloy effectively, the dense $MnCo_2O_4$ layer coating was expected to restrain the low-conductivity $MnCr_2O_4$ spinel phase formation [11, 15].

In this work, dense and conducting ceramic layers with a spinel structure of $MnCo_2O_4$ were deposited by AD on commercial ferritic SS (STS 444). The microstructural changes in the $MnCo_2O_4$/SS interface were analyzed, as were the subsequent electrical conductivity changes, up to 1,000 h at an SOFC operating temperature of 800 °C in air atmosphere.

Experimental procedure

The starting powders were reagent grade $MnCO_3$ and Co_3O_4 (all 99.9% purity, Aldrich, Milwaukee, WI). These oxides were mixed and ball-milled for 18 h in a nylon jar using zirconia balls as the milling media and ethanol as the solvent. The mixed slurry was then dried at ~120 °C and calcined at 1,000 °C for 2 h for $MnCo_2O_4$ spinel phase formation. The calcined powders were ball-milled again to obtain the submicron-size powder appropriate for AD.

The dried, submicron-size powders were mixed with oxygen carrier gas at 99% purity to form an aerosol flow in the aerosol chamber, at a flow rate of 10 l/min. The aerosol flow was transported through a tube to a nozzle, accelerated and ejected from the rectangular-shaped nozzle with orifices of 10 × 0.5 mm^2 into a deposition chamber, which was evacuated by a rotary pump with a mechanical buster. The accelerated $MnCo_2O_4$ particles collided with commercial ferritic SS (STS 444, POSCO, Pohang, Korea), located 5 mm distant from the nozzle. The elemental composition of the STS 444 in weight percentage is Cr 18.59%, Mo 1.96%, Si 0.26%, Mn 0.24%, Ni 0.21%, Al 0.048%, Cu 0.04%, P 0.02%, C 0.006%, and S 0.001%, with the remainder being Fe. The dimensions of the SS substrate were 10 × 10 × 1 mm^3. The $MnCo_2O_4$ ceramics were deposited on both sides of the SS substrate with a thickness of ~3 μm. A schematic figure of this AD equipment has been presented elsewhere [14].

The $MnCo_2O_4$ powders used for AD were characterized by a laser diffraction particle size analyzer (HELOS/BF, Sympatec GmbH, Clausthal-Zellerfeld, Germany). The

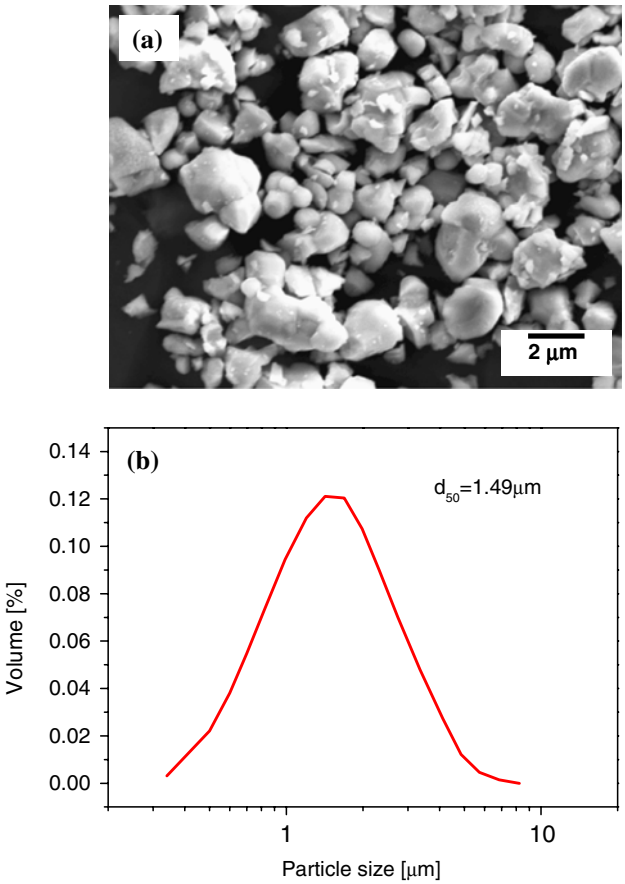

Fig. 1 **a** SEM micrographs and **b** particle size distribution analysis results of the $MnCo_2O_4$ powder used for deposition

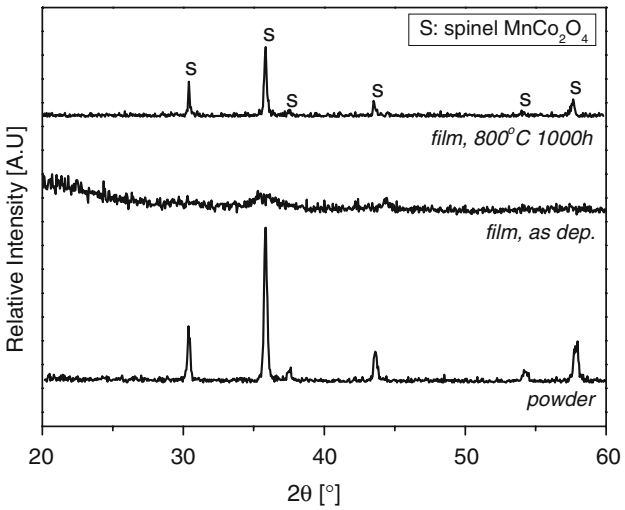

Fig. 2 XRD phase analysis of the $MnCo_2O_4$ powder, as-deposited film and heat-treated film at 800 °C for 1,000 h

crystalline phases of the $MnCo_2O_4$-deposited SSs were identified by X-ray diffraction (XRD, D-MAX 2200, Rigaku, Tokyo, Japan). The powder and film microstructures were observed and the scale compositions were analyzed using a field-emission scanning electron microscope (FE-SEM, JSM-6700F, JEOL, Tokyo, Japan) and scanning

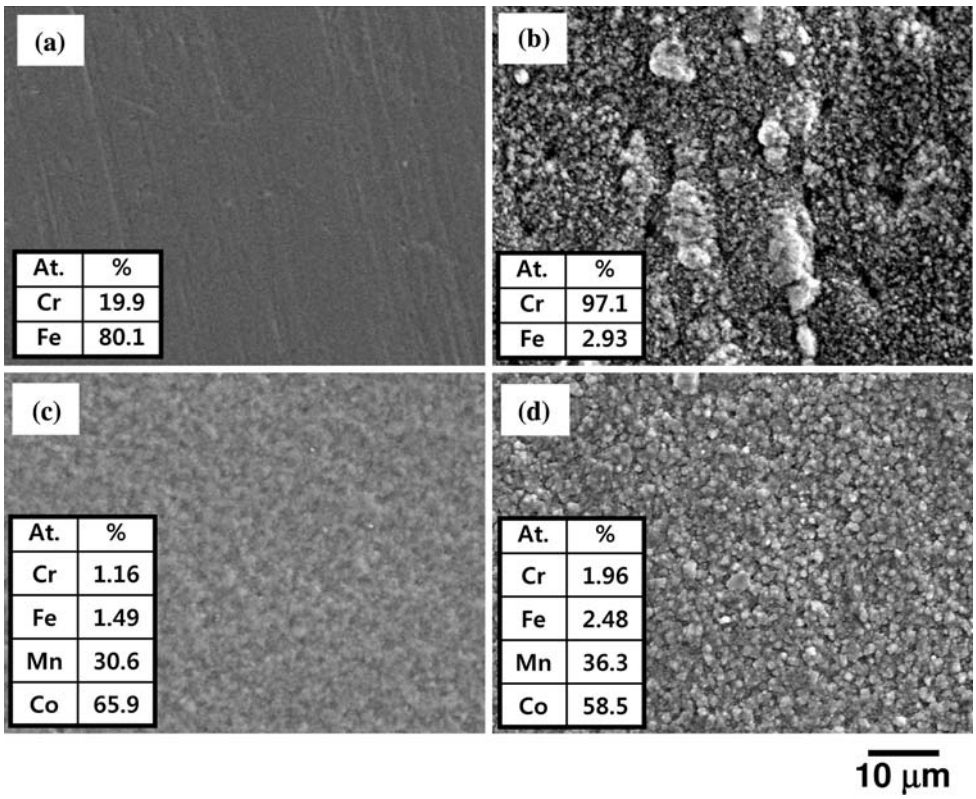

Fig. 3 SEM surface micrographs and EDX quantitative analysis of **a** bare SS, **b** bare SS heat-treated at 800 °C for 1,000 h, **c** $MnCo_2O_4$-coated SS, and **d** $MnCo_2O_4$-coated SS heat-treated at 800 °C for 1,000 h

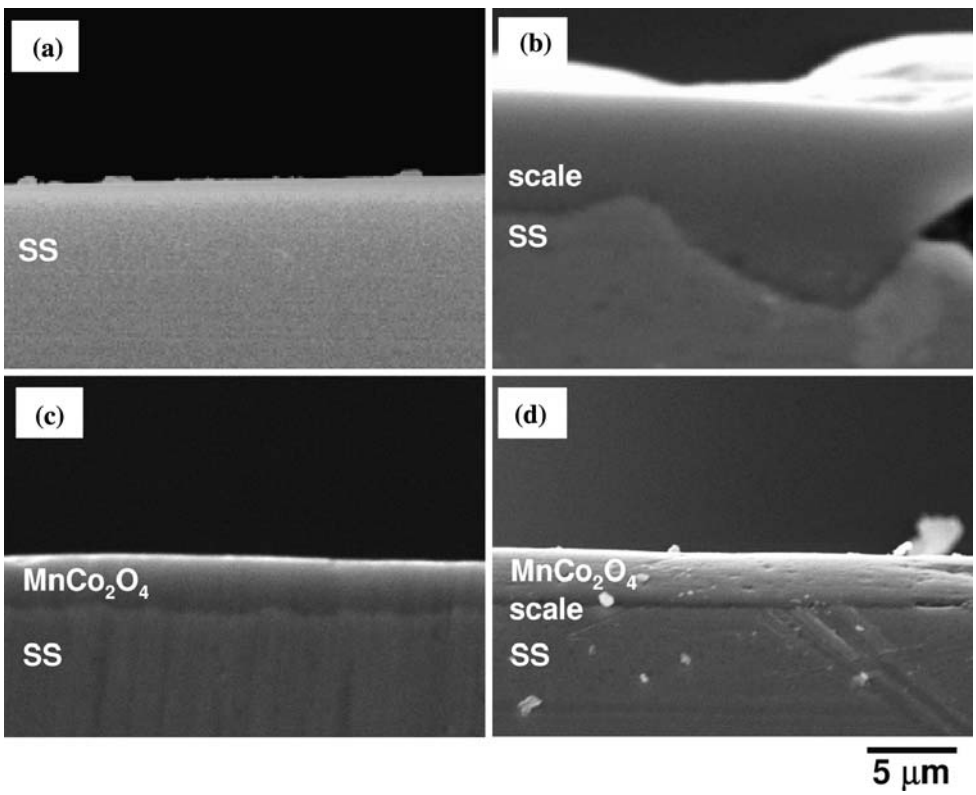

Fig. 4 SEM cross-sectional micrographs of **a** bare SS, **b** bare SS heat-treated at 800 °C for 1,000 h, **c** $MnCo_2O_4$-coated SS, and **d** $MnCo_2O_4$-coated SS heat-treated at 800 °C for 1,000 h

transmission electron microscope (STEM, JEM-2100F, JEOL, Tokyo, Japan) equipped with an energy dispersing X-ray (EDX) system. The ASR of the samples at 800 °C was measured by the 4-probe method with an electrical furnace, with a Pt electrode partially deposited on both sides of the $MnCo_2O_4$-deposited SS sample and Pt wire attached to both sides with a small amount of Pt paste [16]. A current density of 0.1 A/cm^2 was applied during the test, while the voltage was monitored as a function of time, and the linear slope of the current-voltage plot was conserved throughout the measurement.

Results and discussion

Figure 1a and b show the SEM microstructure and particle size analysis results of the $MnCo_2O_4$ powder used for the aerosol flow formation, respectively. The average particle size (d_{50}) of the powder was 1.49 μm. The powder exhibited a spherical shape and unimodal distribution. The XRD phase analysis results of the $MnCo_2O_4$ powder, the as-deposited film on SS using the powder, and the film heat-treated at 800 °C for 1,000 h are shown in Fig. 2. The as-deposited $MnCo_2O_4$ film on SS showed broad peaks due to the nano-crystalline structure formed during the collision of the powders with the substrate, which is a typical characteristic of aerosol-deposited films [10, 12–14]. After heat treatment, the peaks became sharp and the peak intensity was increased due to the crystallization and grain growth, with no phase other than the $MnCo_2O_4$ spinel peaks being observed, probably because the film thickness was larger than the penetration depth of the X-ray wave and no interface scales being detected.

Figure 3a and b show the SEM surface microstructure and EDX quantitative analysis results of the bare SS before and after heat treatment at 800 °C for 1,000 h in air atmosphere, respectively, while Fig. 3c and d show those of the $MnCo_2O_4$-coated SS before and after heat treatment at 800 °C for 1,000 h in air atmosphere, respectively. The SS was fully covered with chromic oxide scales after heat treatment, as shown in the EDX quantitative analysis. However, EDX analysis of the $MnCo_2O_4$-coated SS revealed only a small amount of Cr atomic ratio on the surface and only a slight increase (0.80%, within the error range of EDX quantitative analysis) in the Cr atomic contents after heat-treatment. These observations confirmed the effectiveness of the $MnCo_2O_4$ oxide coating in preventing chromium poisoning of the SOFC stack cathode. The Co atomic ratio was decreased by 7.4% after heat-treatment, while the Mn atomic ratio was correspondingly increased presumably due to the Mn diffusion from the SS substrate [17] or high volatility of the Co atom. Since the conductivity of the $Mn_xCo_{3-x}O_4$ system ($1 \leq x \leq 2$) decreases with increasing x, the Co/Mn ratio decrease was expected to decrease the conductivity of the spinel oxide coating on the SS [18].

The cross-sectional microstructures and compositions of the $MnCo_2O_4$ film interfaces on the SS substrate were observed by SEM and EDX line-scan technique, and the results are shown in Figs. 4 and 5, respectively. Figure 4a–d show the SEM micrographs taken from the polished cross-sections of the bare SS and $MnCo_2O_4$-coated SS samples before and after the heat treatment. For the bare SS samples, a 5- to 10-μm thick oxide scale was formed on the SS surface, but part of the scale was detached and pores were created at the interface after heat treatment, as shown in Fig. 4b. On the other hand, the $MnCo_2O_4$-coated SS exhibited highly dense coating layer and the interface was sharp and clear in as-deposited state, as shown in Fig. 4c. Moreover, the adhesion between the oxide ceramics and SS was well preserved after heat treatment, as shown in

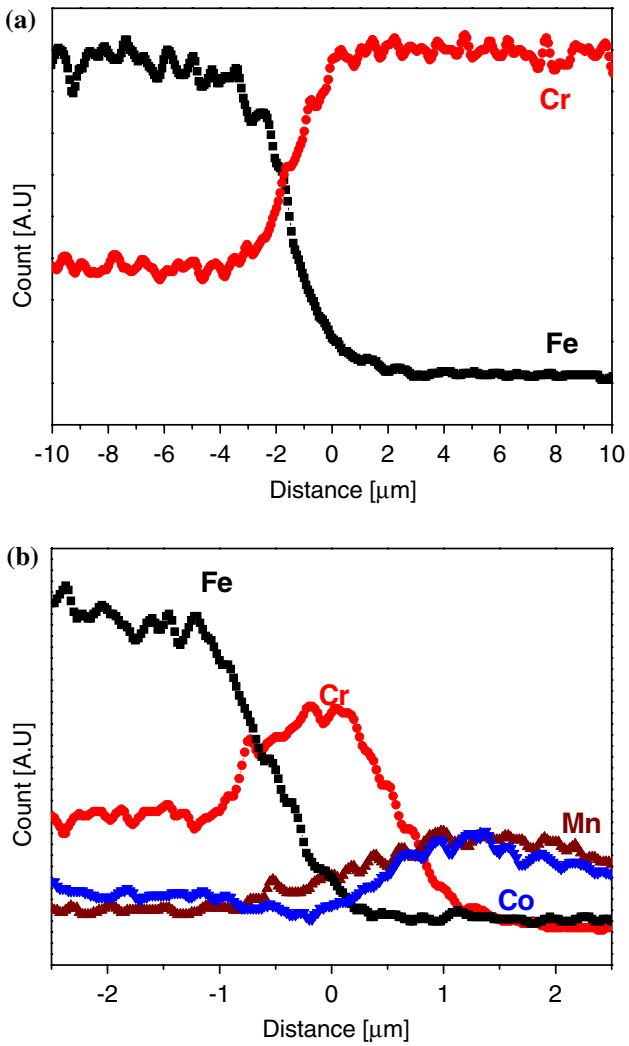

Fig. 5 Compositional profiles by EDX line-scan analysis of **a** bare SS and **b** $MnCo_2O_4$-coated SS heat-treated at 800 °C for 1,000 h

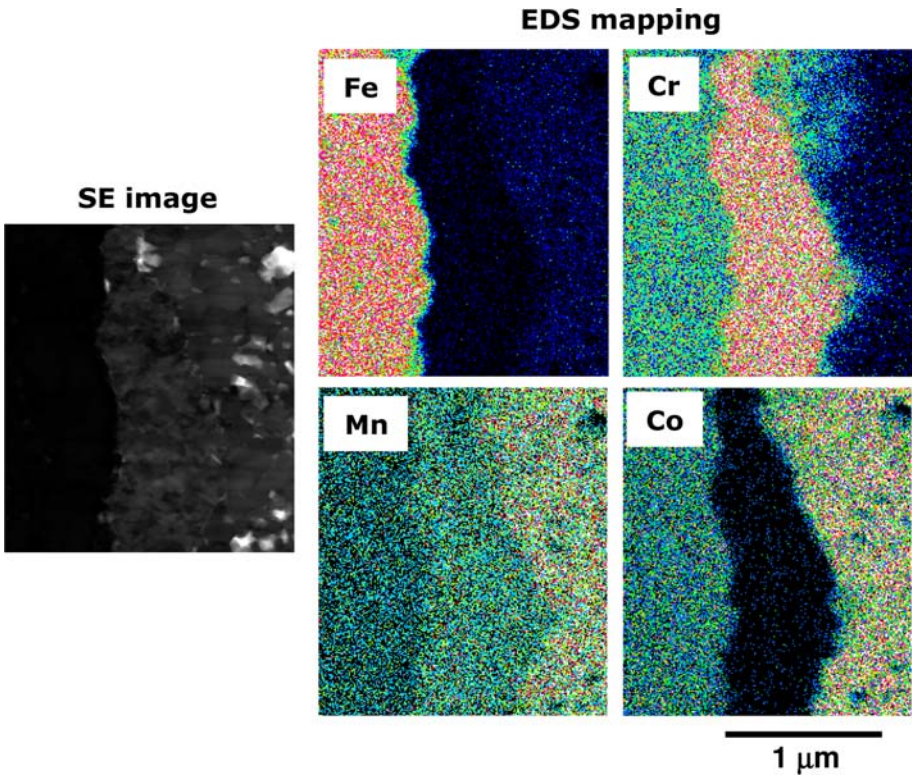

Fig. 6 EDX mapping and STEM image of the interface layer of the $MnCo_2O_4$-coated SS heat-treated at 800 °C for 1,000 h

Fig. 4d. Figure 5a and b show the EDX line-scan graphs of the bare SS and $MnCo_2O_4$-coated SS near the interface region after heat-treatment at 800 °C for 1,000 h. As expected, the bare SS showed a ~10-μm thick, Cr-rich outer-region, while the $MnCo_2O_4$-coated SS showed a sharp Cr increasing region at the interface region with a thickness of ~1 μm, far less than the bare SS.

The interface microstructure was also observed using STEM and the attached EDX mapping equipment. Figure 6 shows the EDX mapping of the Fe, Cr, Mn and Co atoms and the subsequent secondary electron (SE) image in the interface region of the $MnCo_2O_4$-coated SS after heat-treatment at 800 °C for 1,000 h. The interface layer consisted of a Cr-rich layer with a small amount of Mn and Fe. The quantitative analysis results of the interface layer were Cr 97.0%, Mn 1.72% and Fe 1.29%. These results indicated that the interface phase mainly consisted of Cr_2O_3, and that nearly no $MnCoCrO_4$ or $MnCr_2O_4$ spinel phase, which has lower conductivity than $MnCo_2O_4$ spinel phase [15], was formed. In our previous report [12], $MnCr_2O_4$ layer with thickness of ~500 nm was formed between (La,Sr)MnO_3 and Cr_2O_3 scale after heat-treatment at same condition, however, no distinct reaction layer formation was observed between $MnCo_2O_4$ and Cr_2O_3. Figure 7a and b show the STEM micrographs and diffraction patterns of the coated spinel oxide layer and interface scale layer of the $MnCo_2O_4$-coated SS after heat-treatment at 800 °C for 1,000 h, respectively. The crystalline size of the coated spinel oxide layer was 100–150 nm while that of the interface scale layer was smaller. Also, the coated layer showed single spinel phase as shown in diffraction pattern in Fig. 7a, while the interface scale layer seems to be not single Cr_2O_3 phase, as shown in diffraction pattern of Fig. 7b.

Figure 8 shows the variation of ASR with respect to oxidation time over the range 0–1,000 h at 800 °C. ASR of the bare SS increased sharply and reached 86.3 mΩ cm^2 after only 100 h, whereas that of the $MnCo_2O_4$-coated SS showed a gradual increase of ASR values of 13.4 mΩ cm^2 after 1,000 h. The steady ASR increase of the $MnCo_2O_4$-coated SS was probably caused by decrease of Co/Mn ratio and Cr_2O_3 subscale formation; however the increase rate was much lower than that of the bare SS. The low ASR value and slow increase trend were mainly attributed to the stable $MnCo_2O_4$ spinel formation that inhibited low-conductivity Cr-containing spinel phase formation at the interface.

Summary and conclusions

The conducting ceramic layer with a spinel structure of $MnCo_2O_4$ was coated on ferritic SS to suppress the chrome evaporation suppression and retard the Cr-rich scale

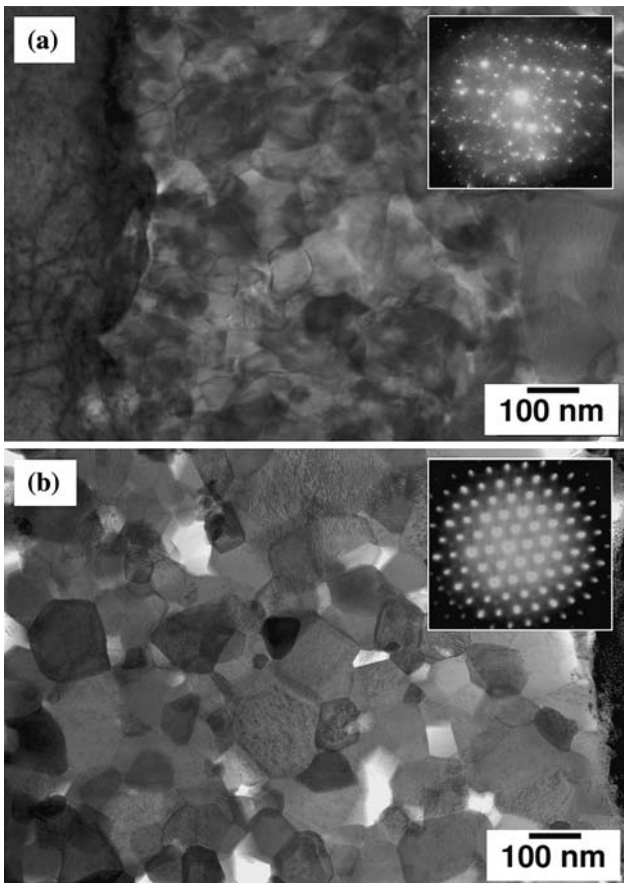

Fig. 7 STEM micrographs and diffraction patterns of the $MnCo_2O_4$-coated SS heat-treated at 800 °C for 1,000 h: **a** coated spinel oxide layer and **b** interfacial Cr-rich oxide scale

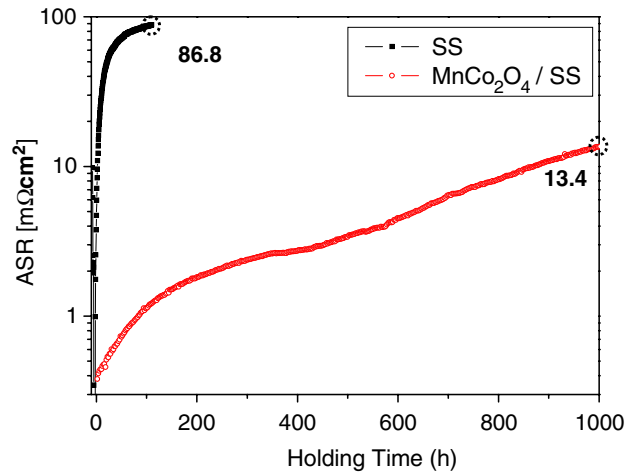

Fig. 8 ASR profiles of bare SS and $MnCo_2O_4$-coated SS according to oxidation time

formation at the operation temperature of SOFC. The ceramic layer coated by AD process was ~3-μm thick, and maintained strong adhesion after heat treatment at 800 °C for 1,000 h. The $MnCo_2O_4$-coated SS showed a surface microstructure with almost no chromic contamination after the heat treatment. A chrome-rich oxide scale was formed at the interface of the $MnCo_2O_4$ and SS. However the thickness was only ~1/10 that of the bare SS, and no Cr-containing spinel phase formation was detected. The ASR of the $MnCo_2O_4$-coated alloys was 13.4 mΩ cm^2 after heat treatment at 800 °C for 1,000 h, while that of the bare SS was ~87 mΩ cm^2 after only 100 h under the same conditions.

Acknowledgement This work was financially supported by the Ministry of Knowledge Economy, Republic of Korea, through the Component-Material development programme.

References

1. Minh NQ, Takahashi T (1995) Science and technology of ceramic fuel cell. Elsevier Science, Amsterdam, The Netherlands
2. Will J, Mitterdorfer A, Kleinlogel C, Perednis D, Gauckler LJ (2000) Solid State Ionics 131:79
3. Zhu WZ, Deevi SC (2003) Mater Sci Eng A348:227
4. Horita T, Xiong Y, Yamaji K, Sakai N (2003) J Electrochem Soc 150(3):A243
5. Simner SP, Anderson MD, Xia G-G, Yang Z, Pederson LR, Stevenson JW (2005) J Electrochem Soc 152(4):A740
6. Yang Z, Xia G, Singh P, Stevenson JW (2006) J Power Sources 155:246
7. Quadkkers WJ, Greiner H, Hansel M, Pattanaik A, Khanna AS, Mallener W (1996) Solid State Ionics 91:55
8. Lim DP, Lim DS, Oh JS, Lyo IW (2005) Surf Coat Technol 200:1248
9. Kim JH, Song RH, Hyun SH (2004) Solid State Ionics 174:185
10. Choi JJ, Lee JH, Park DS, Hahn BD, Yoon WH, Lin HT (2007) J Am Ceram Soc 90(6):1926
11. Yang Z, Xiz G, Simner SP, Stevenson JW (2005) J Electrochem Soc 152(9):A1896
12. Choi JJ, Park DS, Hahn BD, Ryu J, Yoon WH (2008) J Am Ceram Soc 91(8):2601
13. Akedo J (2006) J Am Ceram Soc 89(6):1834
14. Choi JJ, Hahn BD, Ryu J, Yoon WH, Park DS (2007) J Appl Phys 102:044101
15. Chen X, Hou PY, Jacobson CP, Visco SJ, Jonghe LCD (2005) Solid State Ionics 176:425
16. Zhu WZ, Deevi SC (2003) Mater Res Bull 38:957
17. Wu J, Johnson CD, Jiang Y, Gemmen RS, Liu X (2008) Electrochim Acta 54:793
18. Bordeneuve H, Guillemet-Fritsch S, Rousset A, Schuurman S, Poulain V, J Solid State Chem. doi:10.1016/j.jssc.2008.11.004